CONTROL–BASED ACTIVE NOISE CANCELERS FOR DUCTS

M R Bai

National Chiao Tung University, Department of Mechanical Engineering, Hsinchu, Taiwan 30049, R.O.C.

1. INTRODUCTION

Active noise control (ANC) involves the use of loudspeakers and microphones for driving the output of an acoustic plant (a duct in our case) to follow a command signal. Although the realization of ANC systems may differ in forms among systems, a common feature is shared by them [1–7]. The noise from the primary source is detected and then converted to drive the secondary source by a controller. The noise from the secondary source tends to be of equal magnitude and 180° out–of–phase with the noise from the primary source such that the noise level in the downstream field can be reduced.

In this study, several ANC systems are developed on the basis of classical control theory. Each system consists of an open–loop controller that is designed to follow the sound field characteristics (with opposite signs). The residual field in downstream is then fed back to modify the input signal to the open–loop controller through four kinds of feedback controllers. These ANC systems are then realized by analog circuits in accordance with the conceptual design. This basically avoids the the shortcomings of the previously mentioned digital circuit–based systems which require analog to digital (A/D) and digital to analog (D/A) converters with high resolution and conversion rate. Significant reduction of downstream noise level is achieved by using these control–based active noise cancelers, even for broadband random noises.

In the following sections, the principles of the control–based active noise canceler are presented. The procedure of hardware implementation pertaining to four kinds of feedback controllers is explained in details. Then, experiments are undertaken to investigate these ANC techniques. The performance of the ANC systems are compared and the stability criteria are commented.

2. THE CONTROL–BASED ACTIVE NOISE CANCELER

In this section, several kinds of useful control–based active noise cancelers are proposed. Before the entire closed–loop ANC system is formed, an open–loop noise canceler (depicted in Fig. 1) is considered. In the corresponding block diagram (Fig. 2), $H_{ac}(s)$ represents the transfer function from the primary source to the microphone, $H_{bc}(s)$ represents the transfer function from the secondary source to the microphone, and $H_c(s)$ represents the transfer function of the open–loop active noise canceler. $X(s)$ and $E(s)$ denote the source field and the residual field, respectively. The input–output relation of the system can be expressed as

$$X(s)H_{ac}(s) + X(s)H_c(s)H_{bc}(s) = E(s). \qquad (1)$$

In order to suppress the residual field (to ideally zero), the transfer function of the open–loop active noise canceler must satisfy

$$H_c(s) = -H_{ac}(s)/H_{bc}(s). \quad (2)$$

The transfer function $H_c(s)$ can thus be determined from $H_{ac}(s)$ and $H_{bc}(s)$ which should be identified in advance.

Either digital or analog techniques can be utilized to realize the open–loop noise canceler. Operational amplifiers–based analog circuits are used in this study for constructing the ANC systems. In the practical implementation of the ANC system, the frequency responses of the speaker and microphone must be taken into account. The speaker and microphone behave like second–order systems, which introduce magnitude as well as phase distortions to the actual system.

After $H_c(s)$ is calculated according to Eq. (2), the coefficients of the transfer function $H_d(s)$ are extracted by modal testing techniques. Then, the identified $H_c(s)$ can be implemented by analog circuits. It should be noted that, however, $H_c(s)$ does not in general match the real duct characteristics perfectly. There is always some nonzero residual field due to the imperfect $H_c(s)$, especially around the frequencies where the realized $H_c(s)$ does not match well with the real transfer function.

In order to circumvent the problem of nonzero residual field, various types of closed–loop active noise cancelers are thus developed in this study (see Fig. 3). As shown in the corresponding block diagram (Fig. 4), the residual field detected by a downstream microphone is processed by a feedback controller $H_f(s)$. The output from the feedback controller plus the source signal then become the input to the open–loop noise canceler which in turn provides correcting signals to the secondary speaker. The closed–loop active noise canceler can be described by the following equation:

$$E(s) = H_e(s)X(s) + H_c(s)\left[X(s) + E(s)H_f(s)\right] \quad (3)$$

$$E(s)/X(s) = \left[H_e(s) + H_c(s)\right]/\left[1 - H_c(s)H_f(s)\right] \quad (4)$$

For known $H_e(s)$ and $H_c(s)$, the design effort is then focused on the feedback controller $H_f(s)$. The choice of a feedback controller is by no means unique. In this study, four kinds of response compensators from classical control theory are incorporated in the feedback loops of the closed–loop ANC systems [8]:

(a) the proportional (P) feedback controller with the trnasfer function

$$H_f(s) = K_p, \quad (5)$$

(b) the proportional–integral (PI) feedback controller with the transfer function

$$H_f(s) = K_i\,(1 + 1/s), \quad (6)$$

(c) the proportional–derivative (PD) feedback controller with the transfer function

$$H_f(s) = K_d\,(1 + s), \text{ and} \quad (7)$$

(d) the proportional–integral–derivative (PID) feedback controller with the transfer function

$$H_f(s) = K_{pid}\,(1 + 1/s + s). \quad (8)$$

3. EXPERIMENTAL INVESTIGATIONS

3.1 The open–loop active noise cancelers

Prior to the realization of the previously mentioned noise cancelers, the coefficients of $H_c(s)$ associated with the open–loop noise canceler must be calculated, based on the modal

parameters (i.e., natural frequencies, damping ratios, residues) of the actual duct system. This can be done by many modal testing techniques widely–used in the area of mechnical vibration [9]. On the basis of the calculated transfer function results, the open–loop noise canceler is realized by operational amplifier–based analog circuits, including noninverting amplifiers, inverting amplifiers, summing junctions, integrators, differentiators, phase shiftor, and so on [10–12]. The circuits of operational amplifiers (μA 741 in this study) are employed to implement the aforementioned ANC systems. The approach used to construct the open–loop active noise cancelers is termed the direct field canceler.

Referring to the notations in the block diagram of Fig. 2, the transfer function $H_c(s)$ is first calculated by Eq. (2), based on the measured $H_{ac}(s)$ and $H_{bc}(s)$. Then, the characteristics in the duct is identified by modal testing techniques. For the duct used in this study, the transfer function is identified as

$$H_c(s) = \frac{-30.9s - 1442}{s^2 + 54s + 8473} + \frac{-22.5s - 6480}{s^2 + 28s + 90196} + \frac{2.17s - 4175}{s^2 + 20s + 202620} \quad (9)$$

This transfer function $H_c(s)$ is realized by operational amplifier–based circuits, as shown in Fig. 5. The experimental setup of the open–loop noise canceler is shown in Fig. 1. The desired transfer function $H_c(s)$ and the hardware–synthesized $\tilde{H}_c(s)$ are then compared in Fig. 6. Three peaks (100 Hz, 300 Hz, and 450 Hz) can be observed in the figure. The results show that these two transfer functions have nearly identical magnitude gain and 180° phase shift.

The resulting total field due to both the broadband primary source and the secondary source is shown in Fig. 7. Significant attenuation can be observed in the neighborhood of three resonance peaks. The achieved noise reduction of the downstream field is within 5 to 20 dB for the broadband random noise case. The open–loop active noise canceler is also effective for a pure tone primary noise, e.g. a 400 Hz sinusoid. The time–domain and frequency–domain results of the 400 Hz sinusoid are shown in Fig. 8 (in which case the noise reduction of the downstream field is within 20 dB).

3.2 The closed–loop active noise cancelers

As mentioned previously, the residual field in downstream may not be zero due to the imperfect open–loop noise canceler In order to improve the performance of the open–loop noise canceler, the downstream field is fed back to form a closed–loop noise canceler. The block diagram of the closed–loop active noise canceler is shown in Fig. 4, in which diagram $H_f(s)$ denotes the transfer function of the feedback controller. Four kinds of $H_f(s)$ are selected as response compensators in the feedback process.

The first type of the feedback controller $H_f(s)$ employed for construction of the closed–loop active noise cancelers is the proportional feedback controller. The output signal of the feedback controller is made directly proportional to the detected downstream field. The operational amplifier circuit of the feedback controller $H_f(s)$ is shown in Fig. 9.

The power spectrum $\tilde{G}_{ee}(f)$ of the controlled residual field are compared with the uncontrolled field in Figs. 10 (negative K_p) and 11 (positive K_p) to investigate the effects of different gain values. As can be seen from the experimental results, when K_p is positive,

$\tilde{G}_{ee}(f)$ increases around the peak at 450 Hz as K_p increases. On the other hand, when K_p is negative, $\tilde{G}_{ee}(f)$ increases around the peak at 300 Hz as K_p decreases. The noise attenuation of $G_{ee}(f)$ achieved by the proportional feedback controller reaches the maximum at $K_p = -1$.

In order to compare the performance of each active noise canceler in a more quantitative manner, the following performance index is evaluated for each case:

$$\text{Performance index} = \frac{1}{N}\sum_{i=1}^{N}[G_{ee}(f_i) - \tilde{G}_{ee}(f_i)], \qquad (10)$$

where $G_{ee}(f_i)$ demotes the power spectrum of the downstream field at the ith frequency f_i when the secondary source is not present, while $\tilde{G}_{ee}(f)$ denotes the power spectrum of the downstream field when the secondary source is present, and N is the total number of frequency components. The performance index of the P feedback controller is shown in Fig. 12. The three–dimensional hidden–line plot and the contour plot of $\tilde{G}_{ee}(f)$ for different K_p values ranging from –10 to 10 are shown in Fig. 13. These graphic results are particularly useful for identifying the most effective settings of K_p values during the design stage of the active noise cancelers. The performance index is maintained within 6 to 7 dB at the range $-3 < K_p < 3$. The performance index reaches the maximum at $K_p = 1$.

Another important subject of the closed–loop noise canceler is associated with system stability. The root–locus technique is employed to analyze the stability of the closed–loop ANC system with four types of feedback controllers. First, $H_c(s)$ is calculated according to Eq. (2) which yields the identified transfer function, as expressed in Eq. (9). Next, Eq. (5) is utilized to calculate the root loci corresponding to different types of PID feedback controllers for the ANC systems, e.g., the P controller in Fig. 14. The root loci indicate that the stable regions of each closed–loop active noise canceler are $(-\infty, 4)$ for K_p, (0) for K_i, $(-3, 0)$ for K_d, and $(-\infty, 0)$ for K_{pid}. These stability results provide useful guidelines for the design of the ANC systems.

The stability of the P feedback controller is experimentally investigated by incrementally varying the gain K_p. The experimental results are shown in Figs. 10–13. The system is stable when the value of K_p ranges from –4 to 2 and unstable otherwise. It should be pointed out that the discrepancy between the theoretical prediction and the experimental results is mainly due to high frequency resonances of the operational amplifiers. That is, despite the theoretical prediction by root loci, the gain K_p cannot be indefinitely increased because of the inherent hardware restrictions of operational amplifiers.

In addition, similar procedure applies to the other three types of closed–loop active noise cancelers, i.e., PI, PD, and PID feedback controllers. Due to limited space, the detailed discussions are omitted here.

The comparison of the maximum performance index of each control–based active noise canceler is summarized in Table. I. It is observed that the PID feedback controller has the best performance index (6.502 dB), although the differences among these four types of the closed–loop active noise cancelers are almost negligible. By contrast, the performance indices of the open–loop systems are only 3.915 dB for the direct field canceler, which is significantly less than those of the closed–loop counterparts. This again justifies the

necessity of introducing a feedback loop in addition to the open–loop system. The closed–loop controller does provide further improvement to the open–loop active noise canceler, especially when the original open–loop canceler is poorly designed.

4. CONCLUSION

In this research, experimental investigations are conducted to explore various kinds of control–based active noise cancelers for noises in ducts. Operational amplifiers are employed as the building blocks for implementing two types of open–loop and four types of closed–loop active noise cancelers. Extensive experimental results are obtained to demonstrate how well one can construct control–based active noise cancelers.

The closed–loop active noise cancelers provide significantly better noise reduction than the open–loop type because the feedback loop provides frequency response compensation by virtue of residual fields.

The stability predictions of each closed–loop active noise canceler by the root–locus analysis are in good agreement with the experimental investigations. The root–locus analysis provides useful information of stability which might be extremely critical during the design phase of an active noise canceler. Note, however, high frequency resonance of operational amplifiers might also drive the system to unstable regions, which cannot be predicted by the root–locus analysis.

Although the analog circuit–based active noise cancelers prove to be effective for active noise control of noises in ducts, noise cancelers may as well be implemented by digital circuit–based controllers which should provide more flexibility in practical applications. This perspective remains to be explored in the future research.

5. ACKNOWLEDGMENTS

The author is indebted to the graduate student Chiwei Tien for his experimental work throughout the research. The work was supported by the National Science Council in Taiwan, Republic of China under the project number NSC 81–0401–E–009–571.

6. REFERENCES

[1] P Lueg, 'Process of Silencing Sound Oscillators', U.S. Patent No. 2043416 (1936)

[2] M J M Jessel & G A Mangiante, 'Active Sound Absorbers in an Air Duct', *J. Sound Vib.* 23(3) pp393–390 (1972)

[3] M A Swinbanks, 'The Active Control of Sound Propagation in Long Ducts', *J. Sound Vib.* 27(3) pp411–436 (1973)

[4] C F Ross, 'An Algorithm for Designing a Broadband Active Sound Control System', *J. Sound Vib.* 80(3) pp373–380 (1982)

[5] J C Burgess, 'Active Adaptive Sound Control in a Duct:A Computer Simulation', *J. Acoust. Soc. Am.* 70(3) pp715–726 (1981)
[6] A Roure, 'Self–Adaptive Broadband Active Sound Control System', *J. Sound Vib.* 101(3) pp429–441 (1985)
[7] L J Eriksson & M C Allie, 'Use of Random Noise for On–line Transducer in an Adaptive Attenuation System', *J. Acoust. Soc. Am.* 85(2) pp797–802 (1989)
[8] J L Shearer & B T Kulakowski, *Dynamic Modeling and Control of Engineering Systems* (Maxwell–Macmillan, 1990)
[9] D J Ewins, *Modal Testing: Theory and Practice* (John Wiley, 1984)
[10] D F Stout, *Handbook of Operation Amplifier Circuit Design* (McGraw–Hill, 1975)
[11] L M Faulkenbery, *An Introduction to Operational Amplifiers* (John Wiely, 1982)
[12] R A Gayakwad, *Op–amps and Linear Integrated Circuit Technology* (Prentice–Hall, 1980)

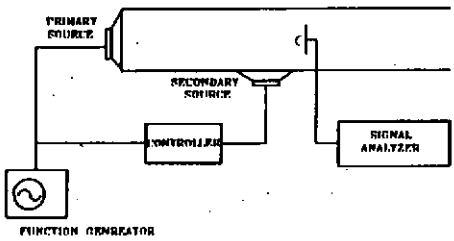

FIG. 1. Experimental setup for the open–loop active noise canceler

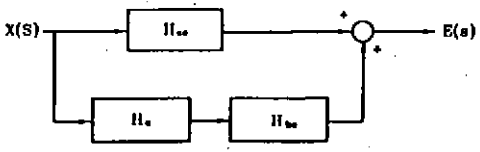

FIG. 2. Block diagram of the open–loop active noise canceler

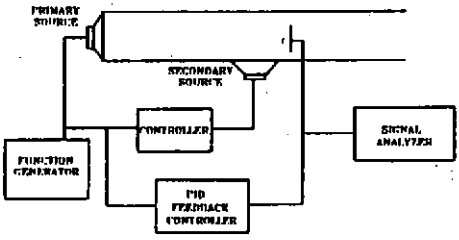

FIG. 3. Experimental setup for the closed–loop active noise canceler

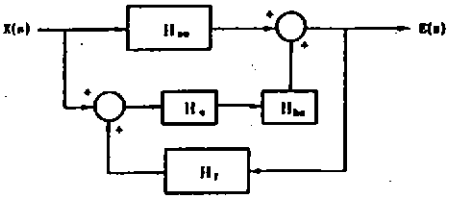

FIG. 4. Block diagram for the closed–loop active noise canceler

ACTIVE NOISE CANCELER

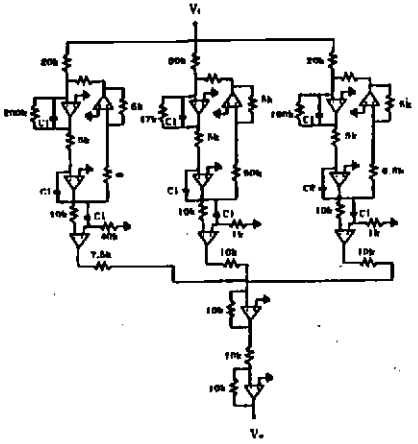

FIG. 5. Operational amplifier circuit of the open-loop active noise canceler H_c ($C1 = 0.1\ \mu F$, $C2 = 0.05\ \mu F$)

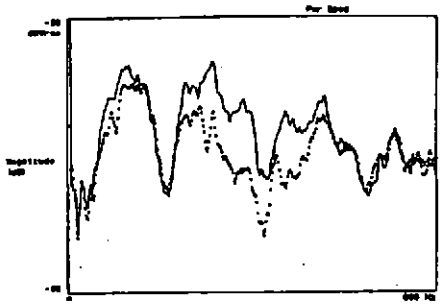

FIG. 7. The power spectrum of the uncontrolled downstream field $G_{ud}(f)$ and the controlled downstream field $G_{cd}(f)$ for the open-loop active noise canceler (— $G_{ud}(f)$, ···· $G_{cd}(f)$)

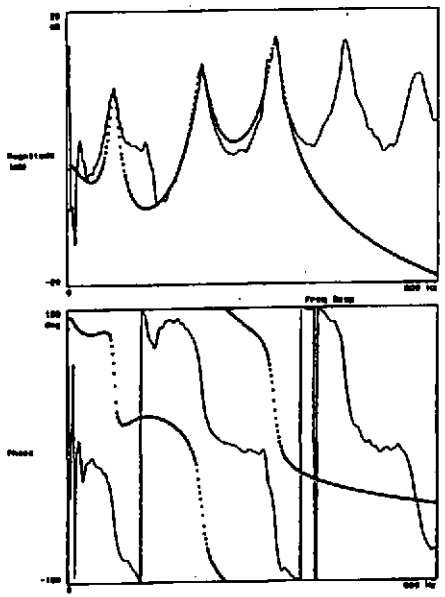

FIG. 6. Comparison of the desired frequency response function of H_c and the analog circuit-synthesized frequency response function H_c for the direct field canceler (— H_c, ···· H_c)

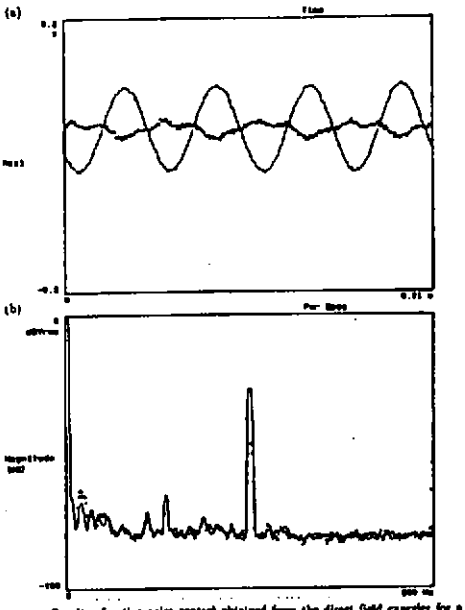

FIG. 8. Results of active noise control obtained from the direct field canceler for a primary sinusoidal noise of 400 Hz. (a) Time domain response: — uncontrolled downstream field, ···· controlled downstream field); (b) frequency domain power spectra: — uncontrolled downstream field, ···· controlled downstream field)

ACTIVE NOISE CANCELER

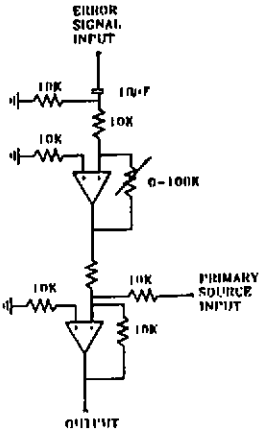

FIG. 9. Operational amplifier circuit for P feedback controller

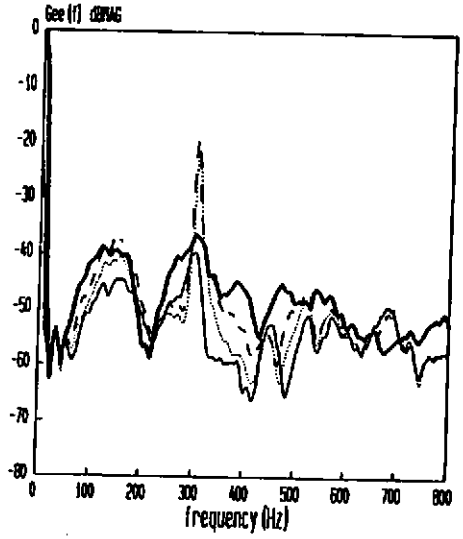

FIG. 10. Comparison of power spectra between the uncontrolled and the controlled downstream fields for the P controller with negative gains. (—— uncontrolled field, —— controlled field when $K_p = -2$, ···· controlled field when $K_p = -4$, — — controlled field when $K_p = -6$)

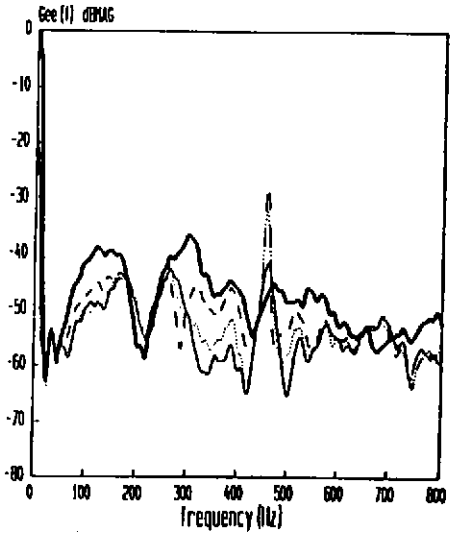

FIG. 11 Comparison of power spectra between the uncontrolled and the controlled downstream fields for the P controller with positive gains. (—— uncontrolled field, —— controlled field when $K_p = 2$, ···· controlled field when $K_p = 4$, — — controlled field when $K_p = 6$)

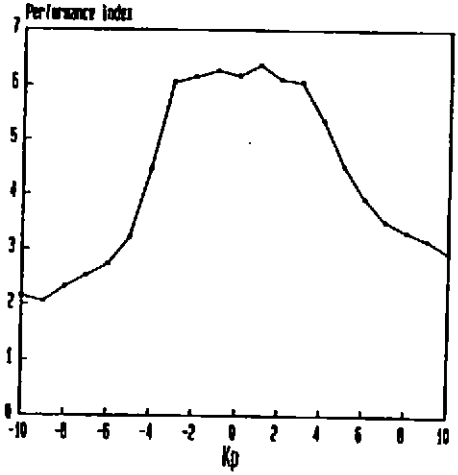

FIG. 12. Performance index for the closed-loop active noise canceler with P controller incorporated in the feedback loop

ACTIVE NOISE CANCELER

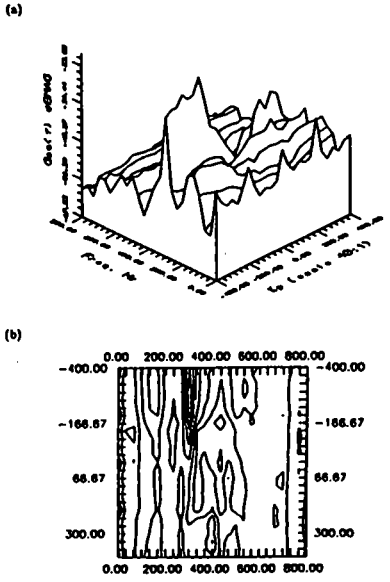

FIG. 13. Downstream residual fields as a function of frequencies and feedback gains when the closed-loop noise canceler with P feedback controller is used. (a) Three-dimensional hidden-line plot; (b) contour plot

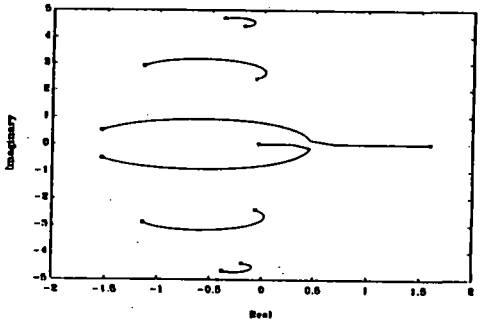

FIG. 14. Root loci of the closed-loop active noise canceler with the P controller. (—— root locus, o root at $K_p = -10$, x root at $K_p = 4$)

TABLE I. Maximum performance indices for different control-based active noise cancelers.

system	feedback	gain	maximum performance index
open-loop	——	——	3.915
closed-loop	P	1	6.372
closed-loop	PI	-1	6.362
closed-loop	PD	-1	6.447
closed-loop	PID	-1	6.502